

Turbulent viscosity by convection in accretion discs – a self-consistent approach

D. Heinzeller^{1,2*}, W.J. Duschl^{2,3} and S. Mineshige¹

¹*Department of Astronomy, Graduate School of Science, Kitashirakawa-Oiwakecho, Sakyo-ku, Kyoto 606-8502, Japan*

²*Institut für Theoretische Physik und Astrophysik, Leibnizstraße 15, 24118 Kiel, Germany*

³*Steward Observatory, The University of Arizona, 933 North Cherry Avenue, Tucson, AZ 85721, USA*

Accepted 2009 April 29. Received 2009 April 26; in original form 2009 March 23

ABSTRACT

The source of viscosity in astrophysical accretion flows is still a hotly debated issue. We investigate the contribution of convective turbulence to the total viscosity in a self-consistent approach, where the strength of convection is determined from the vertical disc structure itself. Additional sources of viscosity are parametrized by a β -viscosity prescription, which also allows an investigation of self-gravitating effects. In the context of accretion discs around stellar mass and intermediate mass black holes, we conclude that convection alone cannot account for the total viscosity in the disc, but significantly adds to it. For accretion rates up to 10% of the Eddington rate, we find that differential rotation provides a sufficiently large underlying viscosity. For higher accretion rates, further support is needed in the inner disc region, which can be provided by an MRI-induced viscosity. We briefly discuss the interplay of MRI, convection and differential rotation. We conduct a detailed parameter study of the effects of central masses and accretion rates on the disc models and find that the threshold value of the supporting viscosity is determined mostly by the Eddington ratio with only little influence from the central black hole mass.

Key words: turbulence – accretion, accretion discs – convection.

1 INTRODUCTION

Modern theoretical modeling of accretion discs dates back to the year 1948, when Weizsäcker published his article about the rotation of cosmic gas (Weizsäcker 1948). A key ingredient to describe the accretion process is the origin of the viscosity, which causes friction in the disc and an inward motion of the material. First observations of accretion timescales of discs in cataclysmic variables invalidated theoretical expectations of molecular viscosity being the driving force (see, e. g., Prendergast & Burbidge 1968; Pringle & Rees 1972). Adversely, they revealed a discrepancy of many orders of magnitude between the numbers measured in the lab and those needed to account for the observations. Soon thereafter, Shakura & Sunyaev (1973) proposed the α -viscosity parametrization, by which most observations could be reproduced satisfactorily. Nevertheless, the Shakura-Sunyaev viscosity remains a purely empirical description and is limited to thin discs with negligible disc masses (i. e., non-selfgravitating discs). Among the physical theories, the most promising ones are:

Differential rotation. An obvious candidate for the turbulence in nearly Keplerian rotating discs is differential rotation. From early laboratory experiments on rotating Couette-Taylor flows (Wendt 1933; Taylor 1936), this possibility was first ruled out.

However, in recent re-investigations, Richard & Zahn (1999) and Richard (2001) concluded that differential rotation can give rise to turbulence, despite published arguments. At the same time, Duschl, Strittmatter & Biermann (1998, 2000) formulated the β -viscosity description. Although being a parametrization like its ancestor, it can actually be related to the process of differential rotation. Contrary to the α -prescription, the β -viscosity accounts properly for the selfgravity of the disc. At the same time, it includes the α -viscosity in the case of a shock dissipation limited, non-selfgravitating disc. Combining the laboratory measurements with the formulation of the β -viscosity leads to a value of $\beta \approx 10^{-5}$ which can be provided by differential rotation.¹

Convection. In order to account for the transport of the energy released by the accretion process, convection is considered to support or even dominate in some cases over radiation and has been studied intensively (Bisnovaty-Kogan & Blinnikov 1977; Shakura, Sunyaev & Zilitinkevich 1978; Goldman & Wandel 1995; Agol et al. 2001) with substantially different conclusions (not least due to the underlying theoretical models): the contribution of convection to the overall energy transport regions ranges from 1/3 (Shakura et al. 1978) to being completely dominant (Bisnovaty-Kogan & Blinnikov 1977) in radiation pressure dom-

¹ As a rule of thumb, $\beta \approx \alpha^2 \dots \alpha$ (Duschl et al. 2000); the corresponding α parameter therefore lies between 10^{-5} and 10^{-3} .

* E-mail: dominikus@kustastro.kyoto-u.ac.jp

inated disc regions. In gas pressure dominated regions, multiple solutions are found in the same range (Goldman & Wandel 1995). Also, recent 2-dimensional simulations by Agol et al. (2001) demonstrate that convective processes can release heat sufficiently fast to modify the vertical structure of the disc. It is therefore natural to consider the turbulence caused by convective motion as a possible candidate for viscosity. First (semi-)analytical investigations were discouraging: they led to discs with masses comparable to or even exceeding the central black hole mass (Vila 1981; Duschl 1989), incompatible with the α -viscosity description assumed in the models. Ruden et al. (1988) and Ryu & Goodman (1992) studied convective instabilities in thin gaseous discs and confirmed that angular momentum transport can be supported by convective turbulence. Goldman & Wandel (1995) investigated accretion discs where viscosity is given by convection solely and where the energy transport is maintained by radiation and convection. They found the resulting viscosity being too low by a factor of 10 to 100, but could not draw final conclusions due to their limited disc model.

Magneto-rotational instability. The magneto-rotational instability (MRI) was first noticed in a non-astrophysical context by Velikhov (1959) and Chandrasekhar (1960). More than 30 years later, Balbus & Hawley (1991, 1998) established that weak magnetic fields can substantially alter the stability character of accretion discs, giving rise to a generic and efficient angular momentum transport. Today, the MRI is considered as the primary candidate for the viscosity in astrophysical accretion flows. Modern computational facilities allow the study of angular momentum transport in magnetized discs in 3-dimensional MHD codes, which basically can be used to calibrate the α - or β -viscosity parameter (see, e. g., Balbus 2005, for a review). The key problem therein is the non-trivial dependency of α on various physical and numerical parameters of the simulations. Recently, Pessah, Chan & Psaltis (2007) presented a scaling law which allows to disentangle physical and numerical influences. The general question if the MRI effects can be translated into an α - or β -type viscosity remains to be answered (see, e. g., Pessah, Chan & Psaltis 2008). From the wealth of results obtained so far, it seems likely that the MRI alone cannot account for the viscosity in astrophysical discs (Begelman & Pringle 2007; King et al. 2007). For example, current results face a discrepancy of at least one order of magnitude between the viscosities generated by the MRI and those inferred from observations (see also Lesur & Longaretti 2007, for a further discussion). A particular problem of the MRI are the so-called *dead zones*, where the growth rate of magneto-rotational instabilities is strongly suppressed and the turbulence induced by magnetic effects diminishes (Gammie 1996). Although the implications of MRI dead zones are discussed mostly for protoplanetary discs (see, e. g., Reyes-Ruiz, Pérez-Tijerina & Sánchez-Salcedo 2003; Brandenburg 2008, for an overview), the overall problem of a vanishing viscosity applies to accretion discs in general.

Thus, it is not yet clear whether one of these candidates or a combination of them is responsible for generating the viscosity in astrophysical discs. One important step therefore is to study the effect of convective turbulence *in combination* with other contributors. Goldman & Wandel (1995) stressed the need for a convective disc model where the vertical structure is calculated self-consistently in order to quantify better the convective turbulence and the energy transport in the disc.

In this paper, we construct a model of a black hole accretion disc where we calculate the effect of convection in a self-consistent way by means of the mixing-length theory. Hereby, the total viscos-

ity is given by convection plus a supporting β -viscosity, accounting for turbulence due to differential rotation and allowing for potential self-gravitating effects. Energy transport in the vertical direction is provided by radiation and convection simultaneously, which allows to derive the strength of the convective viscosity within the model. The details of the model are given in Sect. 2; in Sect. 3, we present and analyse our results for various central black hole masses, accretion rates and values of the underlying β -viscosity. Section 4 is devoted to discussion and conclusion.

2 MODEL SETUP

We calculate accretion disc models where both the viscosity and the transport of energy is supported by convective processes, in addition to an underlying β -viscosity and to radiative energy transport. Hereby, convection is treated in the framework of the mixing-length theory. The disc is assumed to be geometrically thin in order to allow for a 1 + 1-dimensional treatment of the equations. We use a cylindrical coordinate system with planar radial coordinate s , vertical coordinate z and true radius $r = \sqrt{s^2 + z^2}$. The disc geometry is determined by an inner and an outer radius, s_i and s_o , and the disc's thickness $h = h(s)$ from the mid-plane.

The turbulent viscosity, caused by convective processes, is generally given by

$$\nu_{\text{conv}} = \xi v_{\text{conv}} l_{\text{conv}} \quad (1)$$

with v_{conv} and l_{conv} being the turbulent velocity of the convective elements and the convective lengthscale over which they diffuse, respectively. The factor ξ is of the order of unity and depends on the degree of isotropy of convection in the considered direction. For simplicity, we assume isotropy in this investigation (i. e., $\xi = 1/3$). We identify the convective lengthscale l_{conv} with the mixing-length l_m , which will be defined later. We include other sources of viscosity (differential rotation, MRI, ...) by assuming a permanently supporting viscosity to be present in the disc, parametrized by a standard β -ansatz:

$$\nu_{\beta} = \beta s^2 \omega, \quad \beta \ll 1. \quad (2)$$

Here, ω stands for the angular velocity. The total viscosity ν is then given by a combination of these two contributors,

$$\nu = \nu_{\text{conv}} + \nu_{\beta}. \quad (3)$$

2.1 Radial structure

For the calculation of the radial structure, we introduce

$$\Psi = \int_0^h \nu \rho dz. \quad (4)$$

in analogy to the disc's surface density Σ ,

$$\Sigma = \int_0^h \rho dz. \quad (5)$$

Only in the special case of $\nu = \text{const.}$ can we rewrite (4) to $\Psi = \nu \Sigma$. In all other cases, we apply the mean value theorem to define an average value ν^* such that

$$\Psi = \nu^* \Sigma$$

The individual contributors ν^* and Σ remain unknown from the radial structure equations only, but are determined by the vertical structure equations (Sect. 2.2).

The radial structure is determined by the conservation of mass, momentum, angular momentum and energy. The corresponding equilibrium equations are

$$\dot{M} = -4\pi s v_s \Sigma, \quad (6)$$

$$\omega^2 = \frac{g_s}{s}, \quad (7)$$

$$2\Psi = -\frac{\dot{M}\omega}{2\pi s(\partial\omega/\partial s)} \cdot \left(1 - \sqrt{s_i/s}\right), \quad (8)$$

$$2F = -\frac{\dot{M}s\omega(\partial\omega/\partial s)}{2\pi} \cdot \left(1 - \sqrt{s_i/s}\right). \quad (9)$$

\dot{M} denotes the (constant) accretion rate, v_s the accretion velocity with $v_s < 0$ for inflowing material, g_s the gravitational acceleration in radial direction, and F the heat flux, integrated in vertical direction. We apply the standard free-fall boundary condition (Shakura & Sunyaev 1973; Novikov & Thorne 1973) in (8) and (9), implying a vanishing torque at the disc's inner radius s_i . The momentum equation (7) is simplified by the assumption of local equilibrium of the gravitational attraction and the centrifugal repulsion in the radial direction. Therein, the gravitational acceleration is assumed to be given by the monopole approximation (Mineshige & Umemura 1997), assuming a Pseudo-Newtonian gravitational potential (Paczynski & Wiita 1980):

$$g_s = \frac{G(M_c + M_d(s))}{(r - r_s)^2} \cdot \frac{s}{r}. \quad (10)$$

The Schwarzschild radius r_s is given by $2GM_c/c^2$, where M_c denotes the mass of the central black hole. The enclosed disc mass at radius s is calculated via

$$M_d(s) = \int_{s_i}^s 4\pi s' \Sigma ds'. \quad (11)$$

2.2 Vertical stratification

2.2.1 Structure equations

In analogy to Cannizzo & Cameron (1988), Hofmann (2005) and Vehoff (2005), we adopt the energy flux at height z as the independent coordinate for the vertical integration:

$$F_z = \int_0^z \frac{\partial F_z}{\partial z} dz, \quad F_z(z=h) = F. \quad (12)$$

Additionally, we introduce the surface density at height z ,

$$\Sigma_z = \int_0^z \rho dz, \quad \Sigma_z(z=h) = \Sigma, \quad (13)$$

and

$$\psi = \int_0^z \nu \rho dz, \quad \psi(z=h) = \Psi. \quad (14)$$

Neither Σ nor h are known *a priori* – they will be a result of the vertical integration. The equations for the vertical structure of the disc are given as follows:

$$\frac{\partial z}{\partial F_z} = \frac{1}{\rho \nu s^2 \left(\frac{\partial \omega}{\partial s}\right)^2}, \quad (15)$$

$$\frac{\partial T}{\partial F_z} = -\frac{1}{\rho \nu s^2 \left(\frac{\partial \omega}{\partial s}\right)^2} \cdot \left\{ (1-\zeta) \frac{3\kappa \rho F_z}{4acT^3} + \zeta \frac{g_z(4-3\gamma)}{\gamma c_p} \right\}, \quad (16)$$

$$\frac{\partial \Sigma_z}{\partial F_z} = \frac{1}{\nu s^2 \left(\frac{\partial \omega}{\partial s}\right)^2}, \quad (17)$$

$$\frac{\partial p}{\partial F_z} = -\frac{g_z}{\nu s^2 \left(\frac{\partial \omega}{\partial s}\right)^2}. \quad (18)$$

Here, c_p stands for the isobaric specific heat capacity and $\gamma = p_{\text{gas}}/p$. (15) is a simple inversion of the local energy production by viscous dissipation, $\partial F_z/\partial z = \rho \nu s^2 (\partial \omega/\partial s)^2$. The temperature stratification (16) results from accounting for the energy transport by radiation and convection (Cox & Giuli 1968) and using (15). Relating the two terms in (16) with the radiative and adiabatic gradients ∇_{rad} and ∇_{ad} , it becomes clear that the variable ζ describes the relative contribution of the convective energy transport to the total energy transport. Its value depends on the *local* physical conditions at position (s, z) in the disc and can be calculated numerically, see Sect. 2.2.2. Combining (15) with the definition of the surface density at height z (13) leads to (17). Assuming hydrostatic equilibrium and again using (15) gives the last differential equation (18) for the pressure stratification.

Using (16), (18), and the equation of state,

$$p = p_{\text{gas}} + p_{\text{rad}} = \frac{\rho k_B T}{\mu m_H} + \frac{4\sigma_{\text{SB}} T^4}{3c}, \quad (19)$$

we transform (18) into an equation for the mass density ρ :

$$\frac{\partial \rho}{\partial F_z} = \frac{\mu m_H}{k_B \nu s^2 \left(\frac{\partial \omega}{\partial s}\right)^2} \cdot \left[-\frac{g_z}{T} + \left(\frac{p}{\rho T^2} + \frac{4\sigma_{\text{SB}} T^2}{\rho c} \right) \cdot \left\{ (1-\zeta) \frac{3\kappa \rho F_z}{4acT^3} + \zeta \frac{g_z(4-3\gamma)}{\gamma c_p} \right\} \right]. \quad (20)$$

For the numerical solution of the vertical stratification, the opacity $\kappa = \kappa(\rho, T)$ is calculated from a combination of tabulated values and interpolation formulae, see Sect. 2.2.4. In analogy to g_s , the gravitational acceleration in vertical direction g_z is provided by the monopole approximation:

$$g_z = \frac{G(M_c + M_d(s))}{(r - r_s)^2} \cdot \frac{z}{r} + 4\pi G \Sigma_z. \quad (21)$$

In (21), the second term stands for the local gravitational attraction, which becomes important in the self-gravitating regime.

2.2.2 Adaptation of the mixing length theory

In order to solve the vertical structure equations, we apply the mixing-length theory (Böhm-Vitense 1958) as formulated in Cox & Giuli (1968). The mixing-length theory expresses the efficiency of the convective energy transport relative to the radiative transport processes by the variable ζ , where $0 \leq \zeta \leq 1$. A vanishing ζ implies no convective transport, while in the case $\zeta = 1$ all energy is transported by convection. Following Cox & Giuli (1968), its value can be calculated from the cubic equation

$$\zeta^{1/3} + B \cdot \zeta^{2/3} + a_0 B^2 \zeta - a_0 B^2 = 0, \quad (22)$$

with a numerical factor $a_0 = 9/4$ and further quantities defined as

$$\begin{aligned} B &= \left[\frac{A^2}{a_0} \cdot (\nabla_{\text{rad}} - \nabla_{\text{ad}}) \right]^{1/3}, \\ A^2 &= \frac{Q \cdot (c_p \kappa g_z)^2 \rho^5 l_m^4}{288 a^2 c^2 p T^6}, \\ Q &= \frac{4 - 3\gamma}{\gamma}, \\ c_p &= \frac{\mathfrak{R}}{\mu} \cdot \frac{32 - 24\gamma - 3\gamma^2}{2\gamma^2}, \\ \nabla_{\text{rad}} &= \frac{3\kappa \rho \lambda_p F_z}{4acT^4}, \\ \nabla_{\text{ad}} &= \frac{8 - 6\gamma}{32 - 24\gamma - 3\gamma^2}, \\ l_m &= \min(\lambda_p, h), \\ \lambda_p &= \frac{p}{g_z \rho}. \end{aligned}$$

The mixing-length l_m is usually of the order of the pressure scale height λ_p . However, in analogy to the stellar case, it is limited by simple geometric effects. While in the stellar case, it usually cannot exceed the actual radial distance from the centre due to symmetry requirements, we adopt the actual height $h = h(s)$ of the disc as upper limit. In doing so, convective elements are allowed to travel across the disc mid plane, which overrides the symmetry of the disc. Also, it removes the strict upper barrier (i. e., the disc surface) for the convective elements. Nevertheless, it provides a simple method of taking into account overshooting effects and a more realistic, smooth transition between the disc and the atmosphere. We note that the results differ only slightly for a more restrictive definition $l_m = \min(\lambda_p, h - z, z)$, so that our conclusions do not depend on this assumption.

From the above definitions, the cubic equation (22) is solved numerically. Subsequently, the convective viscosity is calculated from (Cox & Giuli 1968)

$$v_{\text{conv}} = c_s \cdot \frac{Q^{1/2} \alpha_{l_m}}{2\sqrt{2}\Gamma_1^{1/2}} \left(\frac{\nabla_{\text{rad}} - \nabla_{\text{ad}}}{a_0 A} \right)^{1/3} \zeta^{1/3}, \quad (23)$$

where c_s denotes the sound speed at the actual coordinate (s, z) in the disc. In the non-relativistic regime, it is given by

$$c_s = \sqrt{\Gamma_1 p / \rho}. \quad (24)$$

The constant Γ_1 stands for the polytropic index, which is given by $5/3$ in the case of a non-relativistic, ideal gas. The parameter α_{l_m} relates the typical distance traveled by the convective elements to the pressure scale height:

$$\alpha_{l_m} = \frac{l_m}{\lambda_p} \leq 1. \quad (25)$$

The derivation of the mixing-length theory assumes a purely subsonic motion of the convective elements, $v_{\text{conv}} \leq c_s$. This inequality cannot be assured by the definition of the convective velocity in (23). Hence, in the case (23) leads to values $v_{\text{conv}} > c_s$, we follow Cox & Giuli (1968) and set manually $v_{\text{conv}} = c_s$. This, in turn, invalidates equation (22) for ζ . Instead, ζ must be calculated from (23) with $v_{\text{conv}} = c_s$:

$$\zeta = \frac{8\sqrt{8}\Gamma_1^{3/2} a_0^{3/2} A}{Q^{3/2} \alpha_{l_m}^3 (\nabla_{\text{rad}} - \nabla_{\text{ad}})}. \quad (26)$$

This correction leads to lower values of ζ and therefore to an effective decrease of the convective energy transport and of the convective viscosity ν_{conv} .

2.2.3 Boundary conditions

We define the boundary conditions for the four equations (15)–(17), (20) at either the disc’s mid plane (“mp”, $F_z = 0$) or surface (“eff”, $F_z = F$):

$$z_{\text{mp}} = z(F_z = 0) = 0, \quad (27)$$

$$T_{\text{eff}} = T(F_z = F) = \left(\frac{F}{\sigma_{\text{SB}}} \right)^{1/4}, \quad (28)$$

$$\Sigma_{z,\text{mp}} = \Sigma_z(F_z = 0) = 0, \quad (29)$$

$$\rho_{\text{eff}} = \rho(F_z = F) = \rho_{\text{eff,input}}. \quad (30)$$

The boundary condition on ρ cannot be determined from the radial structure equations or from simple geometric arguments. It rather requires us to define an atmosphere above the disc, which allows us to determine the density $\rho_{\text{eff,input}}$ consistently with the height h , the surface density Σ and the effective temperature T_{eff} . Details about the atmosphere will be given in Sect. 2.2.5.

2.2.4 Opacity κ

The opacity has a rather strong influence on the computation of the vertical structure. Therefore, we refrain from simple models such as pure electron scattering or Kramer’s law. We rather use a combination of tabulated values and interpolation formulae to calculate the opacity for a broad range of temperatures and densities. The presence of a disc and an atmosphere implies the calculation of Rosseland and Planck opacities.

Tabulated values Given that we want to cover a large domain in temperature and density, multiple sources are included in our model. In the high-temperature limit, we adopt the tables from the TOPS project (TOPS 2008). We compile tables for Rosseland and Planck opacities in the range of

$$\begin{aligned} \log \rho &= [-12.5 \dots +10.5], \\ \log T &= [+4.5 \dots +9.1]. \end{aligned}$$

All values are given in cgs-units. The number of data points is 47 on an equidistant scale for $\log \rho$ and 41 for $\log T$, respectively.

In the low-temperature regime, we include the Ferguson opacities (Ferguson et al. 2005; Ferguson 2008). We compile Rosseland and Planck opacity tables in the range of

$$\begin{aligned} \log R &= [-8.0 \dots +1.0], \\ \log T &= [+2.7 \dots +4.5], \end{aligned}$$

with $R = \rho/T_6^3$ ($T_6 = T/10^6$). These ranges correspond to minimum and maximum mass densities of $\log \rho = -17.9$ and $+6.5$, with a resolution of 19 equidistant points in $\log R$ and 85 in $\log T$.

We choose identical chemical abundances for the TOPS and Ferguson opacities with mass fractions $X = 0.7$, $Y = 0.28$, $Z = 0.02$, and the chemical mixture of Grevesse & Sauval (1998).

Analytic interpolation formula Opacities outside the ranges given above are calculated using an analytic interpolation formula (Gail, priv. comm.; for a similar approach, see also Bell & Lin 1994) for Rosseland opacities. Thus, strictly speaking, this interpolation formula is valid only in the optically thick regions.

Table 1. Interpolation of the opacity: set of parameters (in cgs-units).

Contributor 1	Symbol	$\kappa_{1,0}$	$\kappa_{1,\rho}$	$\kappa_{1,T}$
Dust with ice mantles	κ_{ice}	$2.0 \cdot 10^{-4}$	0	2
Evaporation of ice	$\kappa_{\text{ice, evap}}$	$1.0 \cdot 10^{16}$	0	-7
Dust particles	κ_{dust}	$1.0 \cdot 10^{-1}$	0	1/2
Evaporation of dust particles	$\kappa_{\text{dust, evap}}$	$2.0 \cdot 10^{81}$	1	-24
Molecules	κ_{mol}	$1.0 \cdot 10^{-8}$	2/3	3
Negative hydrogen ion	κ_{H^-}	$1.0 \cdot 10^{-36}$	1/3	10
Bound-free, free-free-transitions	κ_{atom}	$1.5 \cdot 10^{20}$	1	-5/2
Electron scattering	κ_{e^-}	0.348	0	0

$$\frac{1}{\kappa_{\text{in}}} = \left[\frac{1}{\kappa_{\text{ice}}^4} + \frac{T_0^{10}}{T_0^{10} + T^{10}} \cdot \frac{1}{\kappa_{\text{ice, evap}}^4 + \kappa_{\text{dust}}^4} \right]^{1/4} + \left[\frac{1}{\kappa_{\text{dust, evap}}^4 + \kappa_{\text{mol}}^4 + \kappa_{\text{H}^-}^4} + \frac{1}{\kappa_{\text{atom}}^4 + \kappa_{e^-}^4} \right]^{1/4} \quad (31)$$

The individual contributors κ_l are approximated by

$$\kappa_l = \kappa_{0,l} \cdot T^{\kappa_{T,l}} \cdot \rho^{\kappa_{\rho,l}} \quad (32)$$

and are compiled in Table 1. The temperature T_0 parametrizes the transition between atomic/molecular ice and gas and is set to $T_0 = 3000$ K. Note that the definitions of T_0 and of the individual contributors are such that the full interpolation formula (31) fits the values obtained from experiments and numerical calculations; they cannot be used on their own as a physical descriptions of the corresponding processes.

Opacity mixture For smooth transitions and a broad coverage in the T - ρ range, we use a combination of the tabulated opacities (TOPS, Ferguson) and the interpolation formula (31). The transition between the TOPS and the Ferguson opacities takes place at $\log T = 4.5$, modeled by a linear interpolation of the opacities from both sources in the range $\log T = [4.0 \dots 5.0]$.

At the “outer” boundaries of the TOPS- and Ferguson-opacities, we use the same kind of linear transition in a range of $\Delta \log \rho = 1$ and $\Delta \log T = 1$ between the tabulated values and the interpolation formula (31). The resulting opacities are defined on a $\log T$ - $\log \rho$ grid with 150 data points in each direction and

$$\begin{aligned} \log \rho &= [-15.0 \dots +10.0], \\ \log T &= [+1.0 \dots +9.0], \end{aligned}$$

which is sufficient for our purposes. Figures 1a,b display the resulting opacities as a function of temperature for certain densities.

2.2.5 Atmosphere

The only purpose of the atmosphere is to provide a value for the mass density at the surface of the accretion disc at each radial position s , which is consistent with the actual effective temperature, geometrical height and surface density. Therefore, it is sufficient to calculate a simple grey atmosphere in the Milne-Eddington way, where the temperature distribution is given as a function of the optical depth τ by

$$T(\tau)^4 = C_{1,\text{atm}} T_{\text{eff}}^4 \cdot (\tau + C_{2,\text{atm}}). \quad (33)$$

The constants $C_{1,\text{atm}}$ and $C_{2,\text{atm}}$ depend on the transition point τ_{eff} between the atmosphere (optically thin) and the disc (optically thick) and the final value for the temperature at the “upper”

end of the atmosphere ($\tau \ll 1$). We use the common value of $T^4(\tau = 0) = (1/2) \cdot T_{\text{eff}}^4$, but allow the transition to take place at $\tau_{\text{eff}} = 1$ (instead of the common value 2/3) for a simple reason: in the optical thin atmosphere, the equation of state (19) is modified such that the radiation pressure term tends to zero for $\tau \rightarrow 0$. With the approximate expression for the radiation pressure in an optical thin medium (see, e. g., Artemova et al. 1996, for a detailed discussion), the atmospheric equation of state becomes

$$p = p_{\text{gas}} + p_{\text{rad,atm}} = \frac{\rho k_{\text{B}} T}{\mu m_{\text{H}}} + \frac{4\sigma_{\text{SB}}}{3c} \tau T^4. \quad (34)$$

A smooth transition of the pressure between the disc and the atmosphere requires $\tau_{\text{eff}} = 1$, which implies $C_{1,\text{atm}} = 1/2$ and $C_{2,\text{atm}} = 1$. The remaining equations are given as follows: from the definition of the optical depth,

$$d\tau = -\kappa \rho dz,$$

we get an expression for $\partial z / \partial \tau$. The differential expression for the surface density

$$d\Sigma_z = \rho dz$$

is transformed into $\partial \Sigma_z / \partial \tau$. We choose the gas pressure as the fourth dependent variable and assume hydrostatic equilibrium, $\partial p / \partial z = -\rho g_z$, to obtain the following set of differential equations for the structure of the atmosphere:

$$\frac{\partial z}{\partial \tau} = -\frac{1}{\rho \kappa} = -\frac{k_{\text{B}} T}{\mu m_{\text{H}} \kappa p_{\text{gas}}}, \quad (35)$$

$$\frac{\partial \Sigma_z}{\partial \tau} = -\frac{1}{\kappa}, \quad (36)$$

$$\frac{\partial T}{\partial \tau} = T_{\text{eff}} \cdot \left(\frac{1}{2}\right)^{9/4} \cdot (\tau + 1)^{-3/4}, \quad (37)$$

$$\frac{\partial p_{\text{gas}}}{\partial \tau} = \left(\frac{g_z}{\kappa} - \frac{4\sigma_{\text{SB}}}{3c} T_{\text{eff}}^4 \cdot \left(\tau + \frac{1}{2}\right) \right). \quad (38)$$

Equation (37) is derived from the temperature profile (33), and (38) is calculated from

$$\frac{\partial p_{\text{gas}}}{\partial \tau} = \frac{\partial p}{\partial \tau} - \frac{\partial p_{\text{rad,atm}}}{\partial \tau} = -\rho g_z \frac{\partial z}{\partial \tau} - \frac{4\sigma_{\text{SB}}}{3c} \frac{\partial}{\partial \tau} (\tau T^4).$$

The corresponding boundary conditions need to be set at either the lower boundary (i. e., at the disc surface, corresponding to $\tau = \tau_{\text{eff}} = 1$) or the upper boundary (“up”, corresponding to $\tau = \tau_{\text{up}} \ll 1$). Three of these boundary conditions are provided by the solution of the vertical disc structure:

$$h = z(F_z = F) = z(\tau = \tau_{\text{eff}}), \quad (39)$$

$$\Sigma = \Sigma_z(F_z = F) = \Sigma_z(\tau = \tau_{\text{eff}}), \quad (40)$$

$$T_{\text{eff}} = T(F_z = F) = T(\tau = \tau_{\text{eff}}). \quad (41)$$

The fourth boundary condition on the gas pressure has to be set at the upper boundary of the atmosphere, since we want to calculate a consistent value of p_{gas} (i. e., ρ) at the disc surface. We define a constant minimum value for the mass density

$$\rho_{\text{up}} = \rho(\tau = \tau_{\text{up}}) = \text{const.} \quad (42)$$

and calculate the corresponding value $p_{\text{gas,up}}$ at every radial position from $T_{\text{up}} = T(\tau_{\text{up}})$ and ρ_{up} (see Table 2 for the numerical values of ρ_{up} and τ_{up}).

2.3 Numerical solution

Thanks to the 1+1-dimensional model, the radial equations decouple from the vertical structure and can be solved separately. The application of the monopole approximation for the disc’s self-gravity

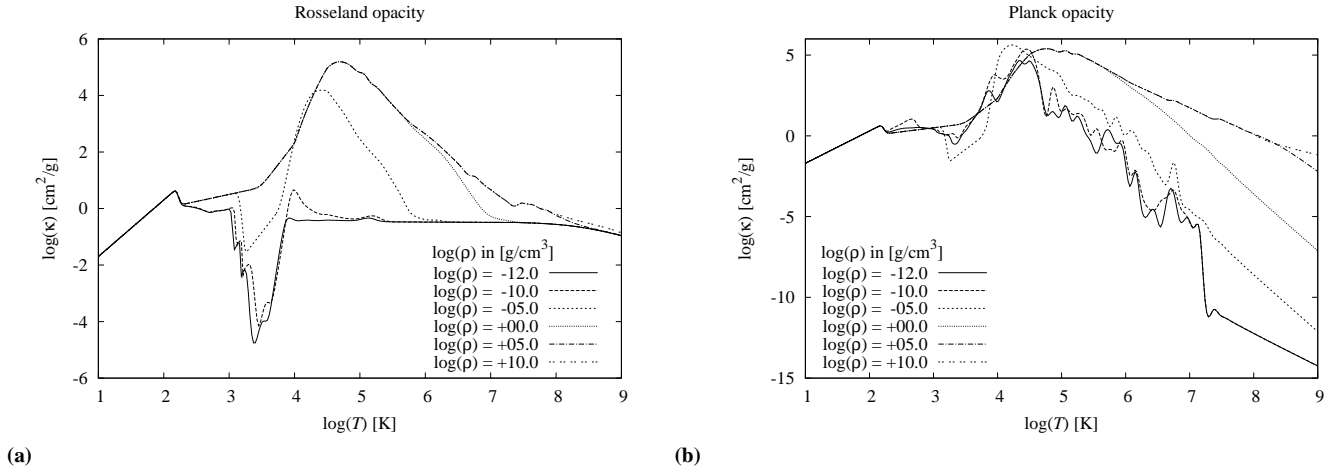


Figure 1. Temperature dependency of the (a) Rosseland and (b) Planck opacities for certain densities

requires the enclosed disc mass M_d at radius s to be known for solving the radial structure equations (c. f. (6)–(9), (10)). A priori, this is only the case at the inner disc radius, where $M_d = 0$. Due to the inner boundary condition, Ψ and F tend to zero for $s \rightarrow s_i$ (c. f., (8), (9)), which causes numerical problems when trying to solve the vertical stratification. Hence, we start the calculation close to the inner boundary, where $M_d \ll M_c$. First, we solve the radial structure equations. With the resulting values of Σ , Ψ and T_{eff} , the vertical structure can be calculated numerically in the second step, allowing to update the enclosed disc mass (11) and to proceed outwards in radial direction.

We use two separate methods to calculate the vertical stratification in the disc and the atmosphere. The disc equations are obviously more complicated to solve and as such they are more prone to numerical issues like, e. g., steep gradients. We therefore apply a Henyey algorithm (Henyey, Forbes & Gould 1964) for solving the set of differential equations in the disc. The Henyey method looks back on a successful history of applications in stellar structure and evolution codes, being able to deal with steep gradients by its relaxation method nature. The atmospheric equations, however, are much easier to solve and do not require a powerful, yet expensive, algorithm like the Henyey method. We apply a standard shooting algorithm to solve the atmospheric structure in a simple and quick way. Details about the numerical methods are presented in Heinzeller (2008).

To determine the consistency of the numerical solution for the vertical stratification at each radius s , we iterate between the Henyey solver for the disc and the shooting method for the atmosphere. Given an initial guess for ρ_{eff} and the boundary conditions (27)–(29), the former one provides values for Σ , h and T_{eff} , once the Henyey solver converged to the correct solution. The latter one updates the input value $\rho_{\text{eff,disc}}$ from the disc solution by solving the atmospheric stratification for the given Σ , h and T_{eff} and the boundary conditions to $\rho_{\text{eff,atm}}$. The combined solution is accepted for

$$|\rho_{\text{eff,disc}} - \rho_{\text{eff,atm}}| \stackrel{!}{\leq} \epsilon \cdot \min \{ \rho_{\text{eff,disc}}, \rho_{\text{eff,atm}} \}, \quad (43)$$

with the required accuracy ϵ being defined in Table 2.

Table 2. Parameters and settings in the numerical model

Central black hole mass	M_c	$1M_\odot \dots 100M_\odot$
Accretion rate	\dot{M}	$0.01\dot{M}_E \dots 0.15\dot{M}_E$
Standard β -viscosity parameter	β	$1 \cdot 10^{-3} \dots 5 \cdot 10^{-6}$
Corresponding α parameter	α	$3 \cdot 10^{-2} \dots 2 \cdot 10^{-4}$
Inner disc radius	s_i	$3r_S$
Outer disc radius	s_o	$500r_S$
Optical depth at upper end of atm.	τ_{up}	10^{-4}
Density at upper end of atmosphere	ρ_{up}	10^{-12}
Grid points in s direction	N_s	100
Default grid points in z -direction	$N_{z,\text{ini}}$	100
Maximum grid points in z -direction	$N_{z,\text{max}}$	210
Max. deviation of disc and atm. sol.	ϵ	0.01

3 RESULTS

The results presented below were obtained for the set of parameters given in Table 2. Due to the free-fall inner boundary condition imposed on (8) and (9), we start the radial calculation at $s = 2s_i = 6r_S$ (see also Sect. 2.3). From the values for the surface density obtained at $s = 2s_i$, we can estimate the enclosed disc mass for $s_i \leq s < 2s_i$, finding that its contribution is more than ten orders of magnitude smaller than the central mass in all cases.

We further verified that in all cases the atmosphere contains almost no mass, compared to the vertical column of the underlying disc. The atmosphere is thin ($z_{\text{min}} \lesssim h$) in the innermost disc region, but expands up to $10h$ in the outer regions due to a significantly smaller gravitational attraction towards the disc mid plane.

3.1 Disc properties of the standard disc model

Our main purpose is to investigate the contribution and efficiency of convection in transporting energy and providing viscosity. We therefore use a standard setup with $M_c = 10M_\odot$ and $\dot{M} = 0.1\dot{M}_E$ for which we vary the β -parameter of the underlying β -viscosity ($\dot{M}_E = 1.67 \cdot 10^{18} \text{ g/s } (M_c/M_\odot)$). We plot the radial structure of these discs in Fig. 2 as a function of radius in units of the Schwarzschild radius $r_S = 2.95 \cdot 10^6 \text{ cm}$.

Common values for the viscosity parameter β are in the range of $10^{-4} \dots 10^{-2}$ (Duschl et al. 2000). To investigate whether the

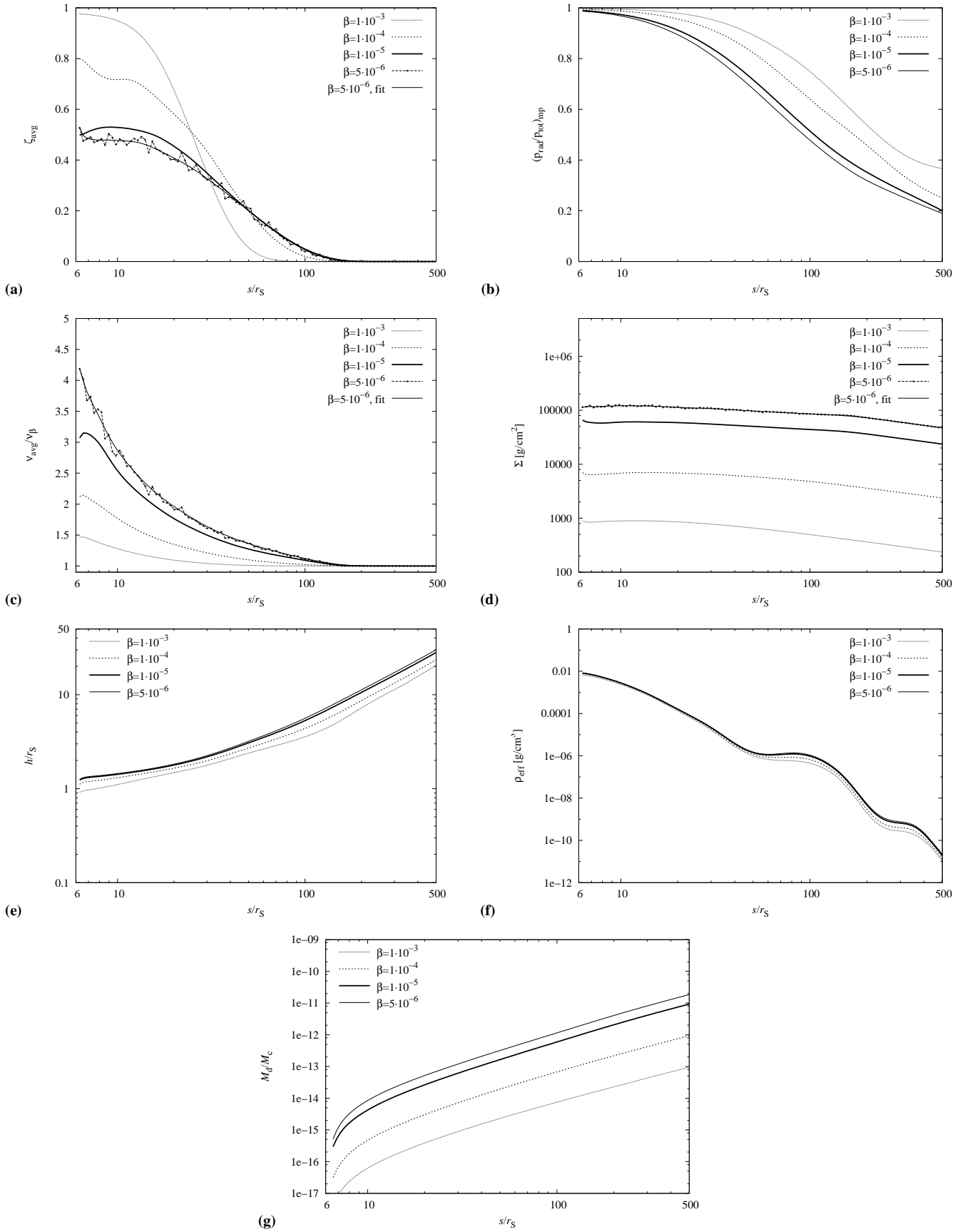


Figure 2. Solutions for the standard disc with $m = M_c/M_\odot = 10$ and $\dot{m} = \dot{M}/\dot{M}_E = 0.10$ for $\beta = [5 \cdot 10^{-6}; 10^{-3}]$

turbulence caused by convection can account partly for the total viscosity, we perform disc calculations with $\beta = [5 \cdot 10^{-6}; 10^{-3}]$. We limit β to this range for the following two reasons.

(i) For $\beta > 10^{-4}$, the standard β -viscosity prescription causes the turbulent velocity $v_{\text{turb},\beta} = \sqrt{\beta} s \omega$ to exceed the sound speed c_s . In that case, a diffusion limit would have to be introduced (Duschl et al. 2000), resulting in an effective decrease of β (see Heinzeller 2008, for a discussion). In the particular example of a $10M_\odot$ black hole accreting at 10% of the Eddington rate, the diffusion limit sets in for $\beta > 1.4 \cdot 10^{-4}$.

(ii) For $\beta < 10^{-5}$, hardly any solutions can be found for the required accuracies and the radial range considered here. The reasons therefore will be revealed hereinafter.

In Fig. 2a, we display the efficiency of convection in the energy transport, measured by the dimensionless quantity ζ . At each radial position, $\zeta = \zeta(s, z)$ is averaged vertically by

$$\zeta_{\text{avg}} = h^{-1} \int_0^h \zeta dz.$$

For $\beta \geq 10^{-4}$, we find that a significant amount of the total energy is transported by convection in the inner part of the disc; close to the inner disc radius, $\zeta \approx 0.98$ for $\beta = 10^{-3}$. Radiative energy transport dominates in the outer part of these discs, with a transition zone expanding from $[10r_s; 80r_s]$ for $\beta = 10^{-3}$ to $[10r_s; 180r_s]$ for smaller β . While the curves show a smooth behavior for $\beta \geq 10^{-5}$, this picture changes when β is decreased further. Radial variations of ζ of about 0.1 occur in the case $\beta = 5 \cdot 10^{-6}$, for which we also plot a fitting curve. In general, smaller supporting viscosities (i. e., smaller values of β) have little influence on the outer regions, while they lead to a significant decrease of the efficiency of convective energy transport in the inner disc region.

For a proper explanation of the possible reasons for these variations in ζ , we display further disc quantities in Figs. 2b–g. The relative contribution of the radiation pressure to the total pressure in the disc’s mid plane is shown in Fig. 2b. A comparison with the efficiency of convection, described by the quantity ζ , nicely confirms theoretical expectations that a strong radiation pressure inside the disc drives the convective motion – a simple linear correlation, however, cannot be found. We would like to point out that both the gas and the radiation pressure do not reflect the instabilities in ζ .

To examine the influence of convective turbulence on the disc viscosity, we further display $\beta_{\text{avg}} = \nu_{\text{avg}}/\nu_\beta$, where ν_β is constant for the vertical stratification and

$$\nu_{\text{avg}} = h^{-1} \int_0^h \nu dz = h^{-1} \int_0^h (\nu_\beta + \nu_{\text{conv}}) dz.$$

In the low- β case, the convective viscosity ν_{conv} becomes three times as large as the underlying β -viscosity. It is important to note that although the convective viscosity becomes *relatively stronger* for lower supporting viscosities, its absolute value decreases as well. As before, instabilities occur for $\beta < 10^{-5}$, which are displayed together with the corresponding fitting curve.

The surface density Σ increases almost linearly with β and reflects the variations of ζ only very weakly. Since the disc scale height h and the density at the disc surface ρ_{eff} are both almost unaffected by the value of β , the increase in Σ is due to a larger internal density in the disc. In all cases, the discs are geometrically thin in the outer part, and “slim” in the inner part, with a maximum ratio of $h/s \approx 0.2$. Contrary to the case of ζ , no instabilities are found in h for the low- β case. The density ρ_{eff} at the disc’s surface shows very similar results for all solutions with a clear decreasing

trend towards larger radii. A certain irregular structure can be seen for all results, an effect of the opacity model, which itself is very sensitive to the densities and temperatures in this region of the disc. As for the pressure and the disc height, the instabilities in ζ are not reflected in the density.

The disc mass M_d increases for decreasing β , but remains completely negligible for all models. We estimate the equality radius s_{equ} where $M_d(s) = M_c$ by extrapolating the results towards larger radii for the $\beta = 10^{-5}$ disc case. A linear fit to the outer region in the log-log plot gives

$$M_d(s)/M_c = 1 \cdot 10^{-11} \left(\frac{s}{500r_s} \right)^{1.75}, \quad \beta = 5 \cdot 10^{-6}, \quad (44)$$

which in turn leads to $s_{\text{equ}} = 6.7 \cdot 10^7 r_s$. Thus, self-gravity is safely negligible in our disc calculations. By means of the radial disc equations (6)–(9), this implies the same results for the total heat flux F and therefore for the temperature T_{eff} at the disc surface (not shown here), regardless of the value of β . Furthermore, this also implies that the radial variations of ζ have no effect on the temperature profile. In summary, the irregularities of the efficiency of convective energy transport are reflected weakly in Σ , but have no influence on the remaining physical quantities.

3.2 Extended parameter space

In this section, we extend the disc calculations towards varying accretion rates and central masses in order to see how general properties and, in particular, the instabilities in ζ , depend on the input parameters.

3.2.1 Eddington ratio \dot{M}/\dot{M}_E

In the first step, we investigate the dependence of the results on the accretion rate while keeping a constant $\beta = 10^{-5}$ and a constant $M_c = 10M_\odot$. We perform disc calculations with accretion rates of $\dot{M} = [0.01; 0.15]\dot{M}_E$. Higher rates are not included, since the discs become too thick for the thin-disc approximation to be valid: for $\dot{M} = 0.15\dot{M}_E$, the ratio h/s reaches values of 0.3 in the inner disc region, while it does not exceed 0.03 for the lower limit $\dot{M} = 0.01$ (see Fig. 3). Furthermore, the same type of radial variations in ζ occur for $\dot{M} > 0.1\dot{M}_E$, which prevent the computations to converge for higher values of the accretion rate. For illustration, we display them along with the fitting curve in Fig. 3a. For the stable solutions ($\dot{M} \leq 0.1\dot{M}_E$), the relative contribution of convection to the overall energy transport is smaller for lower accretion rates. This is because both the total energy and the angular momentum that have to be transported through the disc depend linearly on the accretion rate (c. f., (9), (25)). Thus, the standard β -viscosity is almost large enough to account for both requirements when the accretion rate is low. Higher accretion rates than $0.1\dot{M}_E$ lead to the same type of instabilities of ζ as lower β -values $< 10^{-5}$ do for the standard disc setup ($M_c = 10M_\odot$, $\dot{M} = 0.1\dot{M}_E$). Like in the previous section, a higher convective efficiency corresponds to a higher contribution of the radiation pressure to the total pressure.

Figure 3 further demonstrates that the disc mass and the surface density scale almost linearly with the accretion rate; opacity effects modify this scaling law in case of the density ρ_{eff} at the disc surface. The contribution of convective turbulence is naturally higher the higher the accretion rate is, up to $\nu_{\text{conv}} = 3\nu_\beta$. The convective zone reaches outwards to $20r_s$ for low accretion rates, and to $200r_s$ for high accretion rates, respectively.

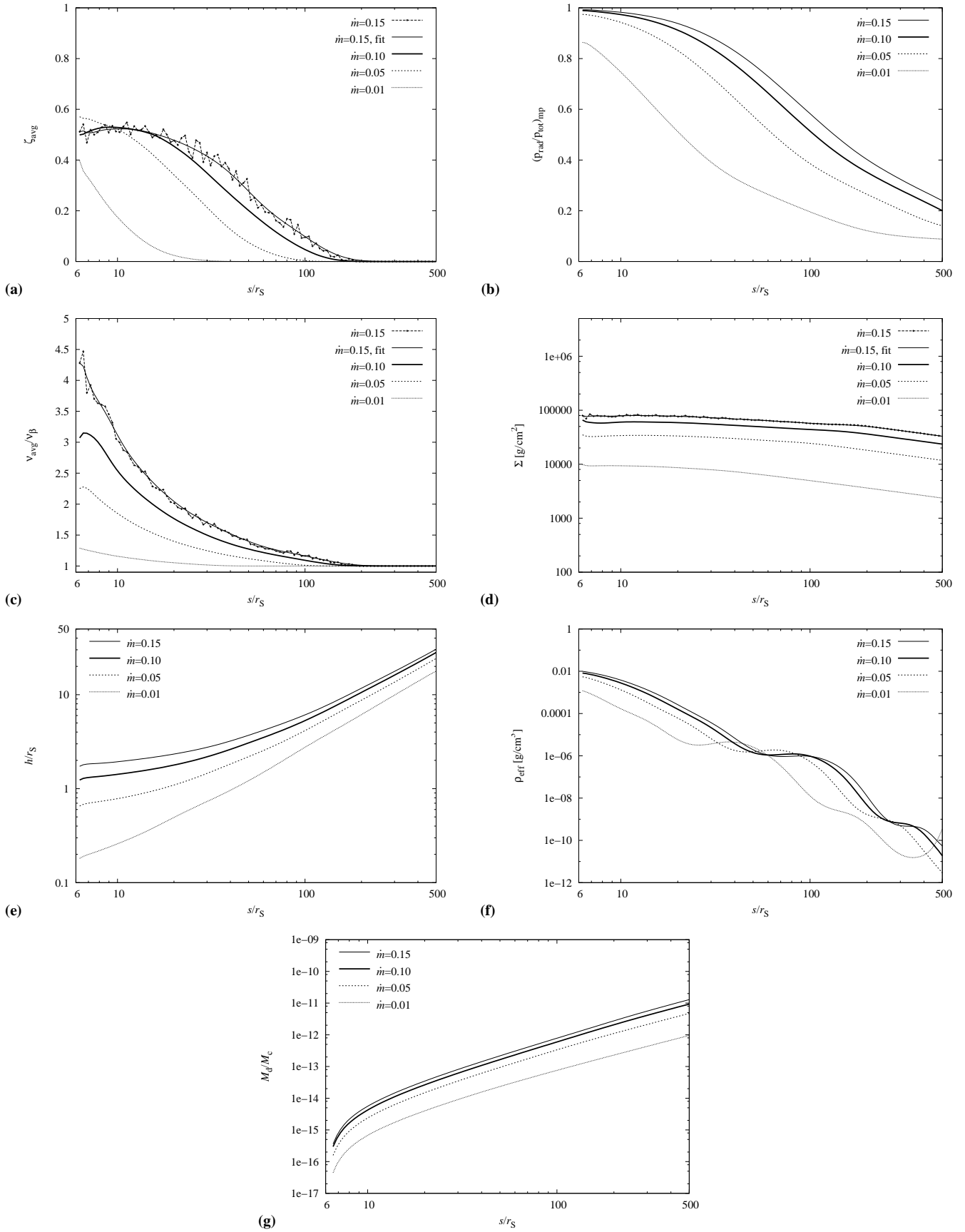


Figure 3. Solutions for varying accretion rates $\dot{m} = \dot{M}/\dot{M}_{\text{E}}$ with $m = M_c/M_{\odot} = 10$ and $\beta = 10^{-5}$

We want to note that the self-gravity of the disc remains negligible and therefore the effective temperature scales with $T_{\text{eff}} \propto \dot{M}^{0.25}$, as expected from the radial structure equations. As in the previous case, the strong variations in ζ are reflected only in the viscosity ν_{avg} and the surface density Σ , though rather weakly.

3.2.2 Central black hole mass M_c

Next, we vary the mass of the central black hole in the range of $M_c = [1; 100]M_\odot$ while keeping a constant $\beta = 10^{-5}$ and a constant Eddington ratio $\dot{M} = 0.1\dot{M}_E$ for the accretion rate. *Thus, the absolute value of the accretion rate is implicitly scaled with M_c .* Figure 4 displays selected properties of these disc models. The efficiency of convection ζ is almost insensitive on a varying central mass, with the small differences being due to the disc temperature (Figs. 4a,c). Depending on the dissipation rate solely, the effective temperature scales with $M_c^{-0.25}$ (see (9)). At the same time, $\nu_\beta \propto M_c$ (see (2)). Thus, less energy has to be transported through the vertical layers, while at the same time the supporting viscosity is increased for higher central masses. Radial variations in ζ set in for the lowest central mass case, $M_c = 1M_\odot$. For completion, we would like to add that the ratio $\nu_{\text{avg}}/\nu_\beta$ is almost independent of the central mass when the Eddington ratio is kept constant, in accordance to the behavior of ζ .

It turns out that both the ratio h/r_S and the surface density Σ do not change for varying central masses. For this fact to hold, the mass density ρ has to scale with M_c^{-1} , which is reflected nicely in Fig. 4b. Then, given that the disc's mass depends only on $s^2 \propto M_c^2$, the ratio M_d/M_c scales with M_c (Fig. 4d). Note that the calculation for the $M_c = 100M_\odot$ case terminates at $s \approx 300r_S$, since the density ρ_{eff} decreases to 10^{-12}g/cm^3 , which is the value of the upper boundary condition ρ_{up} in the atmosphere.

Since the gas pressure ($\propto M_c^{-1.25}$) decreases more rapidly than the radiation pressure ($\propto M_c^{-1}$) with increasing central mass, the ratio $p_{\text{rad}}/p_{\text{tot}}$ is higher the larger the central mass.

3.2.3 Central black hole mass and Eddington ratio

Finally, we investigate the case of varying central masses for a constant $\beta = 10^{-5}$ and a constant absolute value \dot{M} such that it equals $0.1\dot{M}_E$ for a $10M_\odot$ black hole. *Thus, the Eddington ratio \dot{M}/\dot{M}_E scales with M_c^{-1} .* We consider a parameter range of $M_c = [6.7; 100]M_\odot$, corresponding to Eddington ratios of $\dot{M} = [0.15; 0.01]\dot{M}_E$. For even lower central masses (i. e., higher Eddington ratios), the discs get too thick and also the radial variations of ζ become to pronounced to let the calculations converge.

Figure 5 displays selected properties of these discs, which are now controlled by the combined effects of a varying Eddington ratio and central black hole mass. The efficiency of convection, expressed by ζ in Fig. 5a, is determined mainly by the Eddington ratio and is thus similar to Sect. 3.2.1. In the case of the density at the disc surface ρ_{eff} and the temperature T_{eff} (Figs. 5b,c), the two effects enforce each other, while the disc mass M_d is vastly controlled by the central mass and therefore scales as in Sect. 3.2.2 (Fig. 5d).

The pressure ratio $p_{\text{rad}}/p_{\text{tot}}$ shows an inverse behavior than in Sect. 3.2.2, which corresponds to higher convective efficiencies ζ for lower central masses (i. e., higher accretion rates). This inverse behavior is due to the fact that, here, the increase in $p_{\text{rad}} \propto T^4$ is stronger than the increase in $p_{\text{gas}} \propto \rho \cdot T$ for lower central masses.

3.3 Radial variations in the convection efficiency ζ

An important point in this discussion is the origin of the instabilities in ζ for certain disc solutions. We have seen that they occur if the underlying viscosity is decreased under a threshold value, which itself depends on the parameters central mass and accretion rate. Interestingly, these instabilities appear predominantly in ζ and $\nu_{\text{avg}}/\nu_\beta$ and only weakly in the surface density Σ . The effect on the remaining physical quantities is negligible or zero, especially for the observables such as the effective temperature.

Nevertheless, we can understand their occurrence by taking a closer look on the vertical structure in the instable zone of the disc. We therefore plot the vertical stratification of the ratio of the radiation pressure to the total pressure $p_{\text{rad}}/p_{\text{tot}}$, the convection efficiency ζ and the two gradients ∇_{rad} , ∇_{ad} at a radial position close to the black hole, $s = 10r_S$ (Fig. 6). The data corresponds to the case $M_c = 10M_\odot$, $\dot{M} = 0.15\dot{M}_E$ and $\beta = 10^{-5}$, which showed significant oscillations of ζ (Fig. 3). For the horizontal axis, we use the heat flux F_z in units of the total flux F , given by the energy equation (9). The data is taken from a single solution of the vertical structure without any smoothing or averaging.

For reference, we also display the ratio $p_{\text{rad}}/p_{\text{tot}}$ at radial positions $100r_S$ and $300r_S$. Close to the black hole, radiation pressure dominates over gas pressure, while they equal each other at $s \approx 100r_S$. Further outwards, the disc is gas pressure dominated. The average contribution of convection to the energy transport at these positions being $\zeta_{\text{avg}} = \{0.52, 0.1, 0\}$, we conclude that convection is radiation pressure driven and by this confirm the results of Shakura et al. (1978). In all three cases, the vertical layering of the pressure shows smooth curves. Hence, ρ and T must also adopt such a smooth structure and the instabilities in ζ cannot be caused by numerical noise in the density or temperature stratification.

Let us now have a look at the vertical layering of the convective efficiency ζ : we find narrow ‘‘convective cells’’ for small $F_z \approx 0.1F-0.5F$. These small cells are fluctuating for successive iterations (contrary to the extended convective layer between $0.5F$ and F), with the vertical layers close to the mid plane being either fully convective or non-convective. The reason for these fluctuations can be understood from the lower panel of Fig. 6, where we display the two gradients ∇_{rad} and ∇_{ad} , which determine whether convection takes place in the disc: the quantity ζ is determined by the cubic equation (22), which depends strongly on B , with $\zeta \rightarrow 0$ for $B \rightarrow 0$ and $\zeta \rightarrow 1$ for $B \rightarrow \infty$. The key point is that B reflects the Schwarzschild criterium, implying that if the radiative gradient is less or equal to the adiabatic one, the stratification is stabilized and no convection occurs:

$$\nabla_{\text{rad}} \leq \nabla_{\text{ad}} \implies B = 0, \quad \zeta = 0.$$

In the opposite case, even a small positive difference $\nabla_{\text{rad}} - \nabla_{\text{ad}}$ is multiplied by $A^2 \approx 10^{10}$ and therefore $B \gg 1$ and $\zeta \lesssim 1$. Thus, fluctuations in $\nabla_{\text{rad}} - \nabla_{\text{ad}}$, regardless of being of physical or numerical nature, will cause fluctuations in ζ . These fluctuations can not be seen in the physical quantities, because they occur only for small values of F_z and therefore have little effect on the overall structure. For a first interpretation of the physics and a relation to observable quantities, these instabilities play only a minor role and can be replaced by smoothed values. A further investigation of the nature of these fluctuations, however, is necessary in future work. For instance, we find that the results showing radial variations in ζ also show an inversion in the vertical layering of the density. Contrary to the stellar case, it is not clear whether discs are stable when a dominant fraction of the vertical structure is contained within the inversion region (Cannizzo & Cameron 1988).

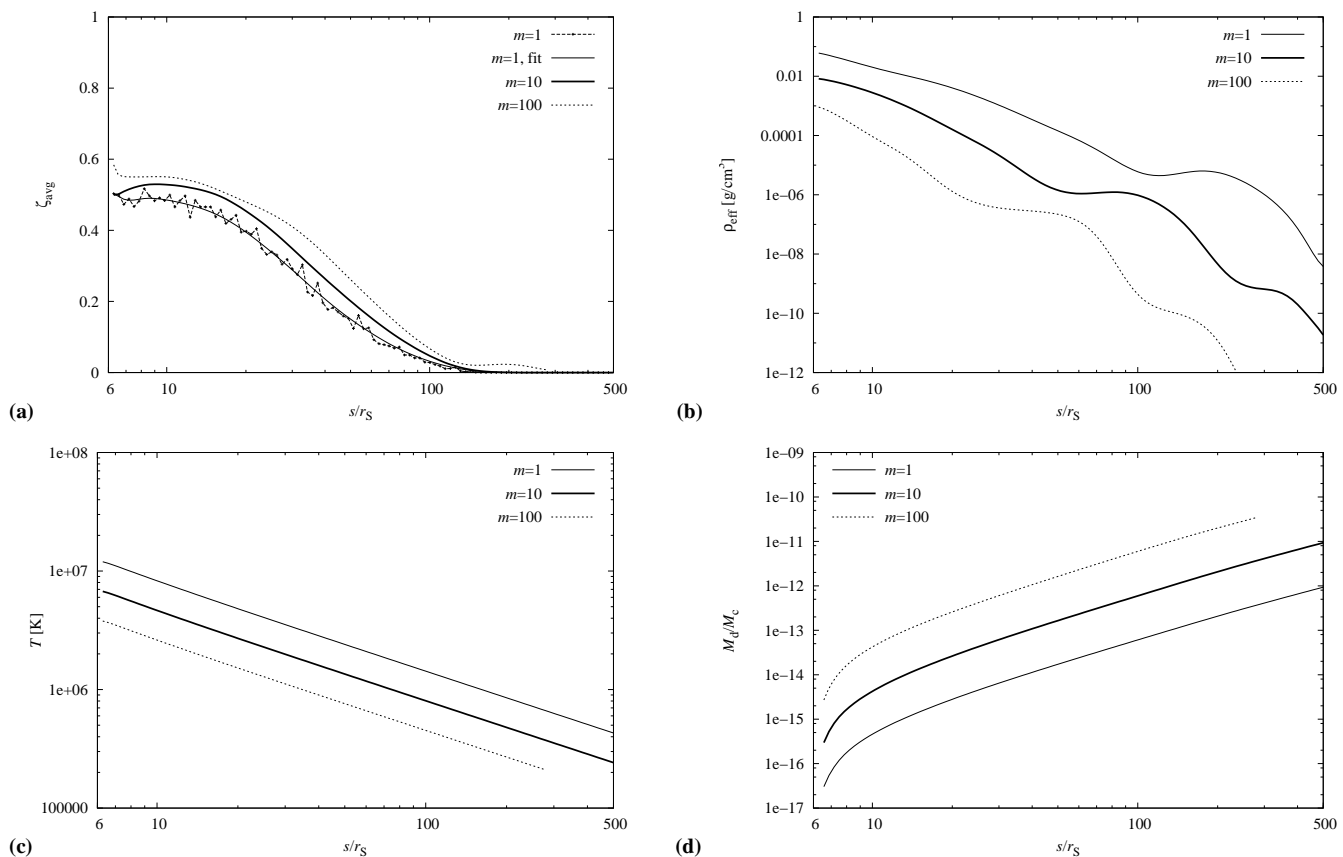


Figure 4. Solutions for varying central masses $m = M_c/M_\odot$, constant Eddington ratio $\dot{m} = \dot{M}/\dot{M}_E = 0.10$ and $\beta = 10^{-5}$

Furthermore, the assumption of hydrostatic equilibrium becomes questionable as soon as the discs are no longer thin and the vertical motion is no longer negligible. With a ratio of up to $h/s \approx 0.3$ for small supporting β -viscosities and for small radii $s < 100r_s$, the resulting discs should be classified as “slim” rather than “thin”. Interestingly, these cases coincide with the solutions showing strong radial variations of ζ . Thus, in accordance to Jiao et al. (2008), waving the assumption of hydrostatic equilibrium and including vertical motion might be important for a more detailed investigation of these irregularities.

4 DISCUSSION AND CONCLUSION

Lower limit on the β -parameter In the light of the above results, we conclude that convection alone cannot account for viscosity in accretion discs. It requires an underlying viscosity, produced by some other process, which is parametrized by ν_β in our model. The reason for this can be understood from the following line of argumentation: convection works towards establishing an adiabatic vertical stratification of the disc. Assuming that there exists an additional source of viscosity in the disc, the convective elements are decelerated by this inherent friction as well and an equilibrium state is established where energy is transported steadily by both radiation and convection, and where the total viscosity is given by the sum of the underlying and the convective viscosity. If, however, the underlying viscosity is too weak, convection is unchecked and very efficient in building an adiabatic stratification in the disc with $\nabla_{\text{rad}} \lesssim \nabla_{\text{ad}}$. In such a *marginally Schwarzschild-stable* state, no

energy is transported and convection ceases. Thus, convective turbulence and viscosity vanish.

In addition, the total viscosity as a result of the vertical integration over $\nu_\beta + \nu_{\text{conv}}$ becomes very small for small values of the supporting β -viscosity. This contradicts the requirements from the radial structure equations: the total amount of energy, released by the accretion process and given by (9), needs to be transported away. Furthermore, viscosity must be present to fulfill the angular momentum transport equation (8). Within this argumentation, the underlying viscosity can also be regarded as the “driving force” for convection.

For low supporting β -viscosities, the density inversion of the vertical layering are more pronounced and at the same time, the disc is no longer thin. A detailed investigation of the vertical structure is needed for a final conclusion about the lower limit for the supporting viscosity. In the limits of this investigation, we conclude that an underlying viscosity is necessary and that its minimum value corresponds to a β -viscosity with $\beta \approx 10^{-5}$. This value agrees well with laboratory measurements of turbulence induced by differential rotation (Richard & Zahn 1999; Richard 2001).

Influence of central mass and accretion rate Our results show that the effects of a varying central mass with fixed *absolute* accretion rate are very similar to those of an inversely varying accretion rate with fixed central mass. With increasing \dot{M}/\dot{M}_E , the required amount of energy and angular momentum that has to be transported through the disc increases, leading to larger threshold values for the total viscosity. Since convection can only partly account for the required increase, the supporting viscosity needs to be larger as well.

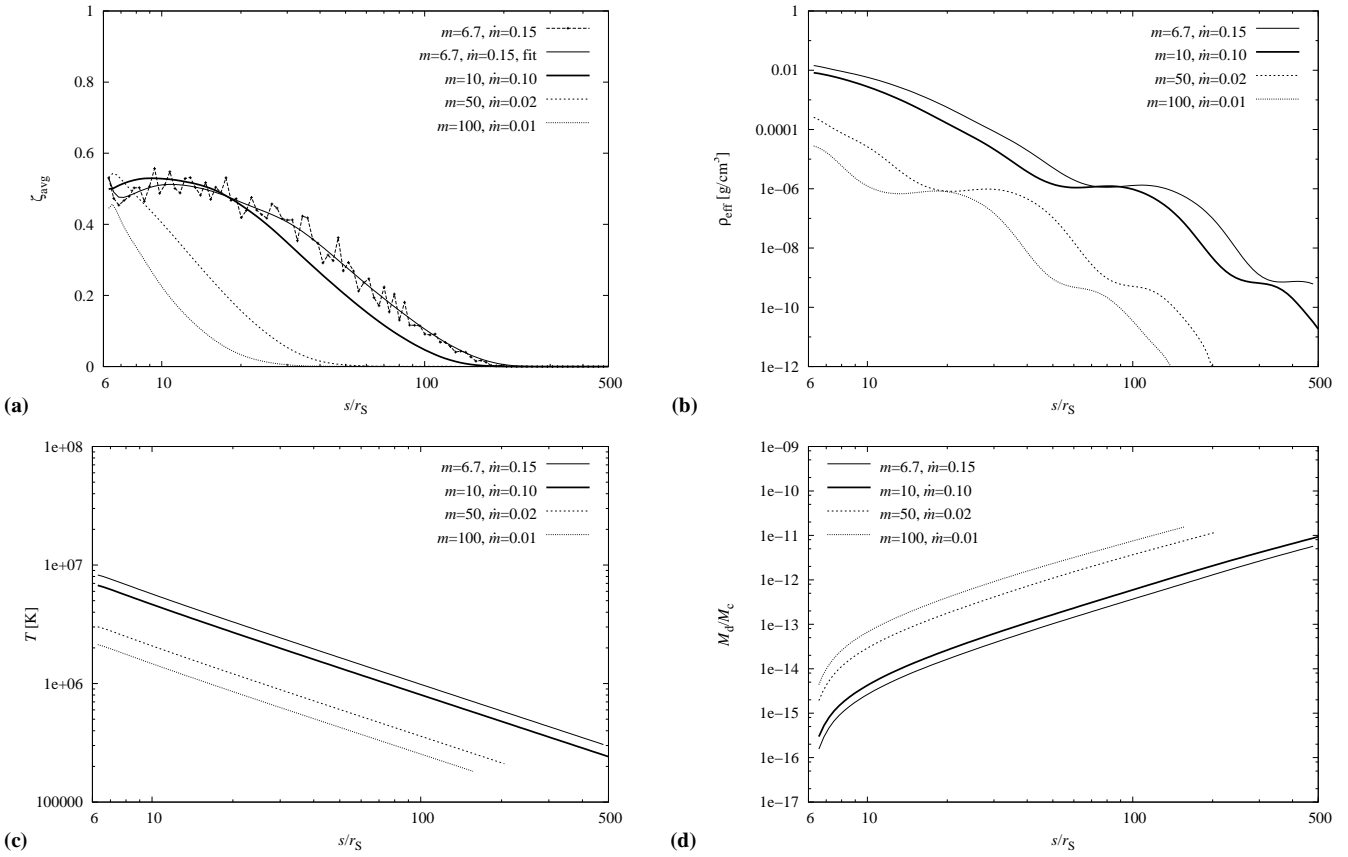


Figure 5. Solutions for varying central masses $m = M_c/M_\odot$ with constant \dot{M} – corresponding to $\dot{m} = \dot{M}/\dot{M}_E = 0.10$ for $m = 10$ – and $\beta = 10^{-5}$

Let us consider the case of a varying central mass while the Eddington ratio is kept constant. Here, changes in M_c have a strong influence on the resulting discs, in particular on the density at the disc surface, the effective temperature and the importance of self-gravity. Figure 4d suggests that we can assume that the radial scaling law (44) for $M_d(s)/M_c$ holds for higher central black hole masses as well. As discussed in Sect. 3.2.2, the ratio $M_d(s)/M_c$ also scales with M_c . Thus, the estimated disc mass at $s = 500r_S$ increases from $10^{-11}M_c$ for a stellar mass black hole with $10M_\odot$ to $10^{-4}M_c$ for a supermassive black hole with 10^8M_\odot , boldly assuming that the extrapolation is valid up to this mass. Correspondingly, the equality radius s_{equ} shrinks by a factor 10^4 . As indicated weakly in Fig. 4a, higher central masses in principle allow for lower supporting viscosities due to the lower temperatures and a relatively stronger supporting β -viscosity (c. f., Sect. 3.2.2).

Convective turbulence, differential rotation and magneto-rotational instability: a speculative viscosity-mixture Our results reveal that disc solutions do only exist if viscosity is also provided by effects other than convection. Convection itself can contribute significantly to the total viscosity, but needs a driving force to establish an equilibrium in energy transport in the vertical direction.

Here, we parametrize the supporting viscosity by a permanent β -viscosity, where the threshold value of the standard β -parameter depends (weakly) on the central mass and (strongly) on the accretion rate. For the case of stellar mass black hole accreting at 10% of the Eddington rate, we find that $\beta \approx 10^{-5}$ is sufficiently large, in agreement with recent laboratory experiments of rotating Couette-Taylor flows.

In this work, we completely ignore the turbulence created by the MRI. Today being regarded as the primary candidate for the high viscosity in accretion discs, some aspects still remain to be clarified (c. f., Sect. 1). For example, as detailed in the introduction, the question whether the viscosity induced by magnetic effects can be translated into an α - or β -type parametrization is still open. Let us assume for the moment that a parametrization is possible. For example, Machida, Nakamura & Matsumoto (2004) investigated the case of an accretion disc around a $10M_\odot$ black hole and found that the corresponding α is not constant, but approximately decreases linearly with radius:

$$\alpha \propto \exp\left\{\frac{1}{2s/r_S}\right\} - 0.99, \quad \alpha \rightarrow 0.01 + \frac{r_S}{2s} \quad \text{for } s \gg r_S.$$

Their results have to be used carefully since the absolute values in the fitting formula depend strongly on the disc corona – a high-temperature and low-density region, put artificially to prevent disc material to evaporate (Machida, priv. comm.). Supposing that the s^{-1} behavior of the MRI viscosity is roughly valid, we can draw the following picture involving differential rotation, convection, and magnetic turbulence: in the inner disc region, convection and differential rotation with a corresponding β -parameter of $\sim 10^{-5}$ alone do not produce a sufficiently high viscosity for the low central mass and/or high accretion rate case. However, close to the central black hole, the magnetic turbulence is strong, resulting in a large viscosity due to the magneto-rotational instability. In the intermediate disc region, a weaker MRI effect adds to convection and differential rotation to account for the required total viscosity. Finally, in the outer disc region, both magnetic effects

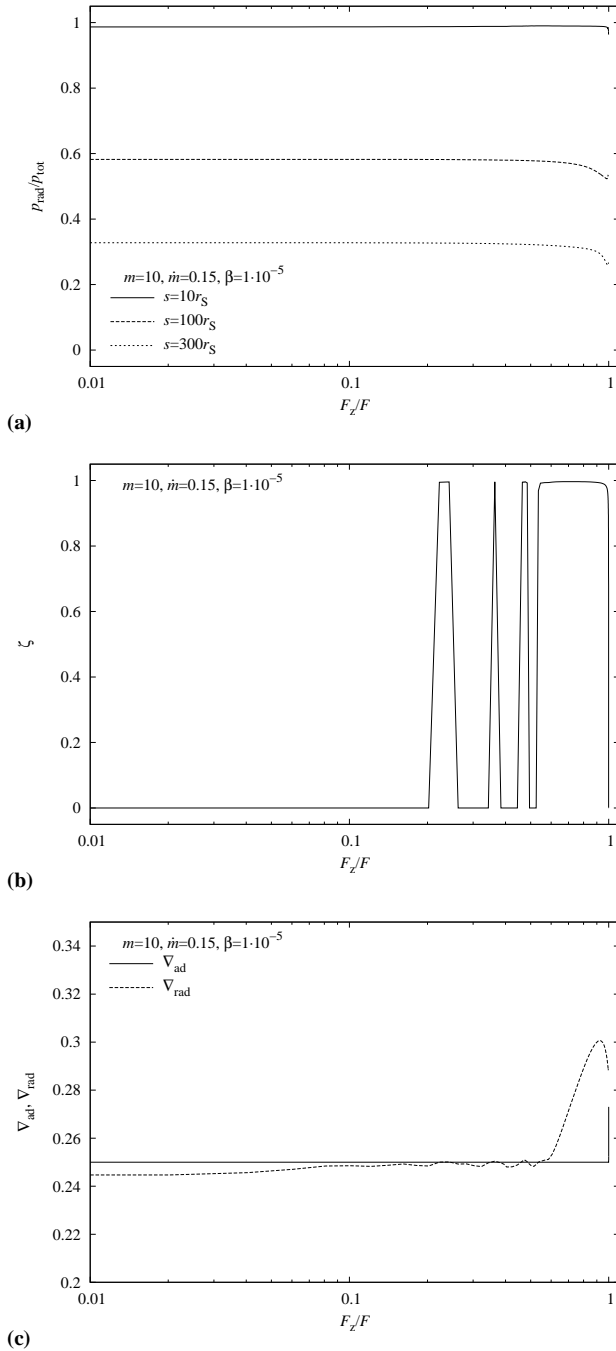


Figure 6. Vertical disc structure close to the black hole at $s = 10r_S$ for $m = 10$, $\dot{m} = 0.15$ and $\beta = 10^{-5}$

and convection become negligible, but differential rotation is sufficient in generating the less demanding values of the total viscosity. An interesting and important investigation therefore would be to combine these three sources of viscosity and to examine whether the required viscosity can be generated for a large variety of disc parameters.

In this study, we applied the mixing-length theory to describe the convective processes in the accretion disc. Although being applied successfully to stellar and accretion disc calculations in the past, this theory has several shortcomings like, e. g., the neglect of radiative losses and rotation or the inability to derive the anisotropy

and the mixing-length within the model. We completely ignored convection in radial direction, which potentially has significant influence on the resulting disc structure through its effects on the radial profile of the mass density, for example. In the case of the thin discs considered here, however, the radial heat flux is negligible and radial convection therefore not important.

In the past, alternative theories for convection in accretion discs have been proposed, although none of them is fully satisfactory. For example, Cannizzo & Cameron (1988) investigated the importance of convective turbulence in cataclysmic variables and compared their results for two different models of convection, the mixing-length theory and a self-consistent theory of convection in accretion discs (Cabot et al. 1987a,b). Their results showed important differences in the efficiency of convection in generating viscosity. The interesting project of an investigation of alternative theories of convection in our disc model is therefore left as future work.

ACKNOWLEDGMENTS

This work was supported by the International Max Planck Research School for Astronomy and Cosmic Physics at the University of Heidelberg (IMPRS HD), by the Grant-in-Aid for the 21st Century COE “Center for Diversity and Universality in Physics” from the Ministry of Education, Culture, Sports, Science and Technology (MEXT) of Japan, and by the Japanese Society for the Promotion of Science (JSPS).

REFERENCES

- Agol E., Krolik J., Turner N.J., Stone J.M., *ApJ*, 558, 543
 Artemova I.V., Bisnovatyi-Kogan G.S., Björnsson G., Novikov I.D., 1996, *ApJ*, 456, 119
 Bisnovatyi-Kogan G.S.; Blinnikov S.I., 1977, *A&A*, 59, 111
 Balbus S.A., Hawley J.F., 1991, *ApJ*, 376, 214
 Balbus S.A., Hawley J.F., 1998, *Rev. Mod. Phys.*, 70, 1
 Balbus S.A., 2005, *ASPC*, 330, 185
 Begelman M.C., Pringle J.E., 2007, *MNRAS*, 375, 1070
 Bell K.R., Lin D.N.C., 1994, *ApJ*, 427, 987
 Böhm-Vitense E., 1958, *Zs. Ap.*, 46, 108
 Brandenburg A., 2008, *Physica Scripta*, 130, 014016
 Cabot W., Canuto V.M., Hubickyj O., Pollack J.B., 1987a, *Icarus*, 69, 387
 Cabot W., Canuto V.M., Hubickyj O., Pollack J.B., 1987b, *Icarus*, 69, 423
 Cannizzo J.K., Cameron A.G.W., *ApJ*, 330, 327
 Chandrasekhar S., 1960, *PNAS*, 46, 253
 Cox J.P., Giuli R.T., 1968, *Principles of stellar structure*, Vol. 1, Physical Principles, Gordon & Breach, New-York-London-Paris
 Duschl W.J., 1989, *A&A*, 225, 105
 Duschl W.J., Strittmatter P.A., Biermann P.L., 1998, 192nd AAS Meeting, #66.17, *Bulletin of the American Astronomical Society*, Vol. 30, p. 917
 Duschl W.J., Strittmatter P.A., Biermann P.L., 2000, *A&A*, 357, 1123
 Ferguson J.W., Alexander D.R., Allard F., Barman T., Bodnarik J.G., Hauschildt P.H., Heffner-Wong A., Tamanai A., 2005, *ApJ*, 623, 585
 Ferguson J.W., 2008, *Research in Low Temperature Astrophysics at Wichita State University*, <http://webs.wichita.edu/physics/opacity/>

- Gammie C.F., 1996, *ApJ*, 457, 355
 Goldman I., Wandel A., 1995, *ApJ*, 443, 187
 Grevesse N., Sauval A.J., 1998, *Space Science Reviews*, 85, 161
 Heinzeller D., 2008, PhD thesis, Univ. Heidelberg,
<http://www.ub.uni-heidelberg.de/archiv/8575/>
 Henyey L.G., Forbes J.E., Gould N.L., 1964, *ApJ*, 139, 306
 Hofmann J., 2005, Diploma thesis, Univ. Heidelberg
 Jiao C.-L., Xue L., Gu W.-M., Lu J.-F., 2008,
<http://arxiv.org/abs/0811.2451v1>
 King A.R., Pringle J.E., Livio M., 2007, *MNRAS*, 376, 1740
 Lesur G., Longaretti P.-Y., 2007, in Bouvier J., Chalabaev A.,
 Charbonnel C., eds, *Proceedings of the Annual meeting of
 the French Society of Astronomy and Astrophysics*, Grenoble,
 France, p. 501
 Machida M., Nakamura K., Matsumoto R., 2004, *PASJ*, 56, 671
 Mineshige S., Umemura M., 1997, *ApJ*, 480, 167
 Novikov I.D., Thorne K.S., 1973, in Witt C.D., Witt B.S.D., eds,
Black Holes Les Astres Occlus, Gordon & Breach, New York, p.
 343
 Paczyński B., Wiita P.J., 1980, *A&A*, 88, 23
 Pessah M.E., Chan C.-K., Psaltis D., 2007, *ApJ*, 668 L51
 Pessah M.E., Chan C.-K., Psaltis D., 2008, *MNRAS*, 383, 683
 Prendergast K.H., Burbidge G.R., 1968, *ApJ*, 151, L83
 Pringle J.E., Rees M.J., 1972, *A&A*, 21, 1
 Reyes-Ruiz M. Pérez-Tijerina E., Sánchez-Salcedo F.J., 2003,
RMxAC, 18, 92R
 Richard D., Zahn J.-P., 1999, *A&A*, 347, 734
 Richard, D., 2001, *Instabilités Hydrodynamiques dans les Ecoule-
 ments en Rotation Différentielle*, PhD thesis, Paris
 Ruden S.P., Papaloizou J.C.B., Lin D.N.C., 1988, *ApJ*, 329, 739
 Ryu D., Goodman J., 1992, *ApJ*, 388, 438
 Shakura N.I., Sunyaev R.A., 1973, *A&A*, 24, 337
 Shakura N.I., Sunyaev R.A., Zilitinkevich S.S., 1978, *A&A*, 62,
 179
 Taylor G.I., 1936, *Proc. Roy. Soc. London A*, 157, 546
 TOPS Astrophysical Opacities: Los Alamos Na-
 tional Laboratory, 2008., *Atomic and Optical Theory*,
<http://www.t4.lanl.gov/cgi-bin/opacity/astro.pl>
 Vehoff S., 2005, Diploma thesis, Univ. Heidelberg
 Velikhov E.P., 1959, *J. Exptl. Theoret. Phys.*, 36, 1398
 Vila S.C., 1981, *ApJ*, 247, 499
 Weizsäcker C.F., 1948, *Z. Naturforsch*, 3a, 524
 Wendt F., 1933, *Ingenieur-Archiv*, 4, 577